



# Fully printed memristors made with MoS<sub>2</sub> and graphene water-based inks†

Zixing Peng,<sup>a</sup> Alessandro Grillo,<sup>ib</sup><sup>a</sup> Aniello Pelella,<sup>b</sup> Xuzhao Liu,<sup>cd</sup> Matthew Boyes,<sup>a</sup> Xiaoyu Xiao,<sup>e</sup> Minghao Zhao,<sup>ib</sup><sup>a</sup> Jingjing Wang,<sup>ib</sup><sup>a</sup> Zhirun Hu,<sup>ib</sup><sup>e</sup> Antonio Di Bartolomeo,<sup>ib</sup><sup>b</sup> and Cinzia Casiraghi,<sup>ib</sup><sup>\*a</sup>

Cite this: *Mater. Horiz.*, 2024, 11, 1344

Received 3rd August 2023,  
Accepted 21st December 2023

DOI: 10.1039/d3mh01224g

rsc.li/materials-horizons

2-Dimensional materials (2DMs) offer an attractive solution for the realization of high density and reliable memristors, compatible with printed and flexible electronics. In this work we fabricate a fully inkjet printed MoS<sub>2</sub>-based resistive switching memory, where graphene is used as top electrode and silver is used as bottom electrode. Memristic effects are observed only after annealing of each printed component. The printed memory on silicon shows low SET/RESET voltage, short switching times (less than 0.1 s) and resistance switching ratios of 10<sup>3</sup>–10<sup>5</sup>, comparable or superior to the performance obtained in devices with both printed silver electrodes on rigid substrates. The same device on Kapton shows resistance switching ratios of 10<sup>2</sup>–10<sup>3</sup> and remains stable at least up to 2% of strain. The memristor resistance switching is attributed to the formation of Ag conductive filaments, which can be suppressed by integrating graphene grown by chemical vapour deposition (CVD) onto the silver electrode. Temperature-dependent electrical measurements starting from 200 K show that memristic behavior appears at a temperature of ~300 K, confirming that an energy threshold is needed to form the conductive filament. This work shows that inkjet printing is a very powerful technique for the fabrication of 2DMs-based resistive switches onto rigid and flexible substrates.

## 1. Introduction

The development of memristic devices capable of storing multiple states of information is required for many applications, ranging from data computation to neuromorphic circuits and adaptive

### New concepts

In this work we demonstrate that water-based graphene and MoS<sub>2</sub> inks, used as top electrode and switching layer, respectively, can be used to realize fully printed memristors with low SET/RESET voltage, short switching times (<0.1 s) and resistance switching ratios of 10<sup>3</sup>–10<sup>5</sup>, comparable or superior to the performance obtained in devices with both printed silver electrodes on rigid substrates. The same device printed on kapton shows resistance switching ratios of 10<sup>2</sup>–10<sup>3</sup> and stable switching up to 2% of strain. Moreover, the devices show temperature dependent memristic behavior, which has never been observed in printed memristors of 2D materials. In addition, our work also provides insights on the filament formation mechanism. For example, we show that by integrating CVD graphene onto the silver electrode enables to completely remove the memristic effect. This work shows that inkjet printing is a very powerful technique for the fabrication of 2DMs-based memristic devices onto rigid and flexible substrates.

systems.<sup>1–4</sup> Research has mostly focused on the improvement of the device performance parameters, such as fast switching speeds, low energy consumption, and high endurance. However, it is also of crucial importance to show integration of such devices onto flexible substrates, enabled by the use of low-cost and mass scalable technologies such as inkjet printing.

2D materials are very attractive for the fabrication of printed memristors as they can be easily processed into inkjet printable formulations and used to fabricate the full device.<sup>5–13</sup> However, very few works have reported fully printed 2DMs-based memristors: most of the literature is based on the use of non-scalable deposition methods such as spin coating or drop casting. In particular, only 3 works have reported printed memristors made of 2DMs,<sup>14–16</sup> while

<sup>a</sup> Department of Chemistry, University of Manchester, Oxford Road, Manchester, UK. E-mail: cinzia.casiraghi@manchester.ac.uk

<sup>b</sup> Physics Department “E. R. Caianiello”, University of Salerno, via Giovanni Paolo II n. 132, Fisciano, 84084, Salerno, Italy

<sup>c</sup> Department of Materials, University of Manchester, Oxford Road, Manchester, UK

<sup>d</sup> Photon Science Institute, University of Manchester, Oxford Road, Manchester, UK

<sup>e</sup> Department of Electrical and Electronics, University of Manchester, Oxford Road, Manchester, UK

† Electronic supplementary information (ESI) available: State of art of memristors tables; silver electrode thickness and best printing passes; optical image, *I*-*V* curves and RS ratio of memristors with different Ag electrode width; *I*-*V* curve of FS devices; RS ratio of STS and FS devices; summary of Ag/MoS<sub>2</sub>/Gr devices table; profilometry, SEM, XRD and XPS of Ag/MoS<sub>2</sub>/Gr memristors; electrical properties of non-volatile Ag/MoS<sub>2</sub>/Gr memristor; *I*-*V* curves of Ag/MoS<sub>2</sub>/Gr memristors on Kapton; *I*-*V* curves for Gr/MoS<sub>2</sub>/Gr devices; calculation of the filament temperature; temperature dependence *I*-*V* measurements; integration of CVD graphene, including fabrication of the CVD inserted device, UV-vis, Raman study and *I*-*V* curves of different structure CVD inserted devices. See DOI: <https://doi.org/10.1039/d3mh01224g>





thickness of the silver film is found to be also important in the optimization of the device fabrication: if the silver film is too thick, cracks appear in the MoS<sub>2</sub> film (Fig. S1, ESI<sup>†</sup>), which is printed on top of it, leading to devices with no resistive switching (RS) behavior.

All devices were made with a step-by-step (STS) annealing, where each film of the heterostructure was annealed after printing (see Experimental section for more details). Fig. 1b shows the electrical characteristics of the device obtained at a current compliance of 10<sup>-4</sup> A: a clear threshold-type volatile RS behavior is observed, *i.e.* the memristor abruptly switches from a high resistance state (HRS) to a low resistance state (LRS) beyond a threshold voltage, associated to the “SET process”, and then shows resistance recovery when the bias is removed, no matter the polarity of the sweep voltages. Fig. 1c shows the *I*-*V* curves measured over 10 cycles. However, when we apply a continuous sweep voltage, the switching characteristic turns into a non-volatile behavior, as shown in Fig. 1d. In this case, after setting the memristor in LRS with a switching voltage of ~5 V, a voltage bias with opposite polarity is required to make a RESET process, *i.e.* to bring the memristor to HRS.

As the memristic effect is expected to be caused by migrations of silver ions and formation of conductive filaments, the overlapped area between the silver electrode, the dielectric layer and the top electrode is expected to affect the performance of the device. Hence, the overlapped area has been changed by varying the width of the Ag film from 0.1 mm to 0.5 mm. The optical images of the devices are shown in Fig. S2 (ESI<sup>†</sup>). Fig. S3 (ESI<sup>†</sup>) shows that the Ag/MoS<sub>2</sub>/Gr memristors achieve higher RS ratio with a relatively small active area. This seems to be counterintuitive, however one should consider that the uniformity of the silver film is expected to decrease by increasing the printed area, for example some pin-holes are visible on the widest silver films (Fig. S2, ESI<sup>†</sup>). Overall, the device with 0.2 mm width Ag bottom electrode shows the best performance, amongst all devices investigated (Fig. S4, ESI<sup>†</sup>).

We also compared two different annealing processes: STS and final-step (FS) annealing, in which the device was annealed only once, and after printing of all components. Fig. S5a (ESI<sup>†</sup>) shows the *I*-*V* curves measured over 10 cycles for a Ag/MoS<sub>2</sub>/Gr device made with FS annealing: only hysteresis is observed. Fig. S5b (ESI<sup>†</sup>) shows the memristor performance, reported as the RS ratio, defined as the resistance ratio between the current measured at the LRS and HRS ( $I_{\text{LRS}}/I_{\text{HRS}}$ ) for all the Ag/MoS<sub>2</sub>/Gr memristors, fabricated with different geometries (see ESI<sup>†</sup>, Table SIII for full details on the devices geometry) and divided by type of annealing. Note that in Fig. S5b (ESI<sup>†</sup>) we normalized the Ag/MoS<sub>2</sub>/Gr memristors by the active area. This figure shows that STS annealed memristors are more likely to achieve RS ratio above 10<sup>2</sup>. A maximum RS of 10<sup>5</sup>-10<sup>6</sup> can be achieved, if the device is properly optimized. In contrast, the memristic effect is hardly visible when FS annealing is used, with RS ratio of 10<sup>2</sup> achieved only for a few devices.

In order to further investigate the effect of annealing on the memristic behavior, we performed profilometry, cross-sectional scanning electron microscopy (SEM), X-ray diffraction (XRD)

and X-ray photoelectron spectroscopy (XPS). However, we did not observe any strong change in the elemental composition and structure of the films, before and after annealing (Section S4, ESI<sup>†</sup>), in the limit of the experimental resolution. Since pyrene melting temperature is ~400 °C, while glycol propylene, Triton-X and Xanthan gum melt at 200-270 °C, annealing at 150 °C is expected to remove mainly residual water from the film. Previous studies on printed capacitors<sup>31</sup> have shown that STS annealing allows to better remove residual water from the film, hence enabling to measure the dielectric constant of printed h-BN films. Based on these observations, we can conclude that the removal of water molecules somehow affects the memristic behavior, *i.e.* STS annealing is needed to see memristic effects in our device because this process is more efficient than FS annealing at removing the residual solvent from the printed film. Furthermore, it is likely that the printed film may have also a slightly different morphology when subjected to the different types of annealing but this cannot be resolved with traditional characterization techniques. It is clear that both the morphology and the presence of additional molecules trapped in the film are crucial to obtain devices with memristic effects, *i.e.* the structure and composition of the film affect the formation of the silver filament. Therefore, we predict that by finely controlling the morphology, porosity and composition of the printed dielectric film (*e.g.* amount of residual solvent), the RS ratio could be even further improved.

Fig. 2a shows a pulsed voltage test on the optimized Ag/MoS<sub>2</sub>/Gr memristor. A voltage of 4 V was applied with 1 second pulse (ON/OFF time). After applying the pulsed voltage for a total of 30 s, the device reaches the SET condition, by switching on in just 0.1 s (Fig. S10, ESI<sup>†</sup>). The relatively rapid RS capability enables fabrication of non-volatile Ag/MoS<sub>2</sub>/Gr memristors. Fig. 2b summarizes the SET and RESET voltages of 50 memristors. It can be seen that all devices are working, but due to the non-uniformity of the inkjet printing devices, the SET and RESET voltages are distributed in a small range, with the most frequent SET voltage seen at about +2 V, while the RESET voltage is slightly smaller, at around -1 V. To note that a voltage switching range from ±1.4 to ±5 V has been observed in devices that have been proposed for integration of 2D based memristor in CMOS technology.<sup>32</sup>

We have also conducted up to 100 cycles of rapid testing and examined the stability of the optimized memristor in both HRS and LRS, finding that the device can keep switching for over 100 cycles and remains stable in both HRS and LRS for at least 10<sup>4</sup> seconds with negligible degradation. The estimated lifetime of the memristors in the LRS state is about 1000 hours (Fig. S11, ESI<sup>†</sup>). Fig. S12 (ESI<sup>†</sup>) shows that the switching speed of the memristors increases when the voltage applied between the two electrodes is increased, so as the ON/OFF ratio of the device. The higher voltage is expected to speed up the migration of Ag ions in the MoS<sub>2</sub> dielectric layer and to promote the rapid switching of the memristors. The memristor can set in few seconds even when narrow pulses voltage ( $\Delta t = 0.5$  s and 0.6 s) are applied. In particular, with a set voltage of 3V, the memristor can switch for over 100 cycles, as shown in Fig. S13 (ESI<sup>†</sup>).



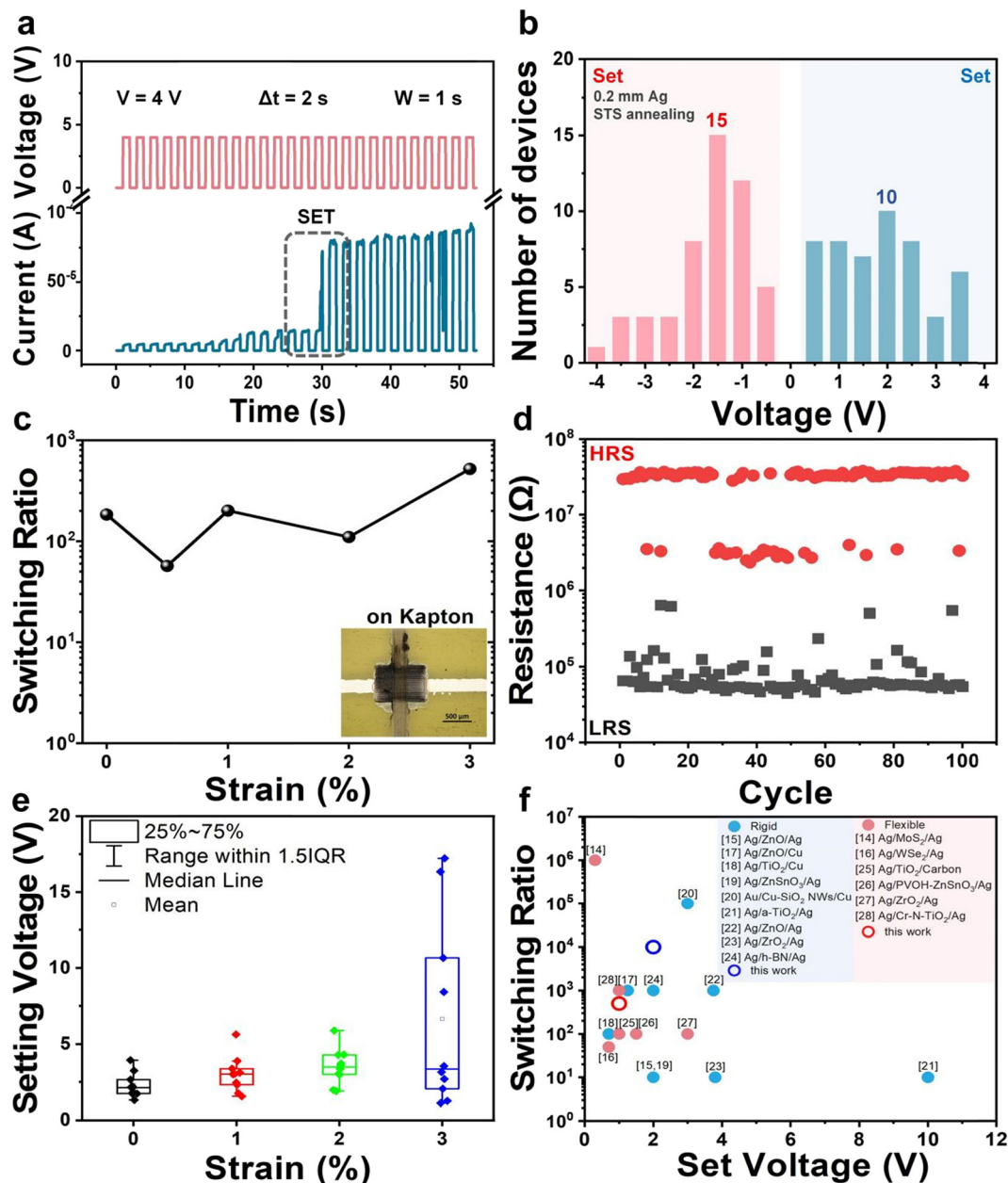


Fig. 2 Switching behavior of the Ag/MoS<sub>2</sub>/Gr memristors. (a) The current response from input voltage pulses generated by the Ag/MoS<sub>2</sub>/Gr device, made with STS annealing. (b) Statistical distributions of V<sub>SET</sub> over 50 devices. (c) Resistive switching characteristics of the Ag/MoS<sub>2</sub>/Gr memristors printed on Kapton. Inset: Optical image of a printed devices on Kapton. (d) Cycle endurance test of a single Ag/MoS<sub>2</sub>/Gr on Kapton. (e) Switching voltage measured on 10 Ag/MoS<sub>2</sub>/Gr devices printed on Kapton under bending at different strain. (f) Benchmarking of the fully printed Ag/MoS<sub>2</sub>/Gr memristor compared to state-of-the-art printed memristors fabricated on rigid and flexible substrates.

Since our devices are fabricated by inkjet printing, they can be easily integrated onto flexible substrates. The inset in Fig. 2c shows the optical image of a fully-printed Ag/MoS<sub>2</sub>/Gr memristor printed on Kapton. Fig. S14 (ESI<sup>†</sup>) shows its *I*-*V* characteristics over 10 cycles: each cycle shows stable memristic behaviour. Fig. 2c shows the results of a bending test: the RS ratio remains around 10<sup>2</sup> up to strain of 3%; Fig. 2d and Fig. S15 (ESI<sup>†</sup>) shows that the RS ratio of the pristine and strained (under 1% and 2% strain) Ag/MoS<sub>2</sub>/Gr memristors on Kapton remains between 10<sup>2</sup>-10<sup>3</sup> for over 100 cycles. Fig. S16 (ESI<sup>†</sup>) shows the LRS and HRS

and the *I*-*V* characteristics of a Ag/MoS<sub>2</sub>/Gr memristor that has been bent for 500 times with a bending radius of 2.5 mm (corresponding to 1% strain) and 1.25 mm (corresponding to 2% strain). Both devices show similar switching characteristics of the pristine (*i.e.* unbent) device printed on Kapton. The bending endurance is comparable to most of the reported values for printed memristors (ESI<sup>†</sup>, Table SII(b)). This demonstrates the suitability of the devices for flexible and printable electronics. The switching voltage of the device under bending conditions has also been reported in Fig. 2e, including statistical analysis



(see full set of data in ESI† Table SV), showing good reproducibility of the performance parameters for strain up to 2%. Finally, Fig. 2f compares the RS and the set voltage of our printed memristors with fully printed memristors based on various nanomaterials from the state of art (see ESI† Tables SI and SII). When printed on rigid substrate, our devices show the highest RS for a SET voltage below 2 V; on flexible substrate, our devices show performance comparable to most of the printed memristors reported in literature made with silver electrodes.

In silver-based ECM memristors, the RS mechanism is explained by the Ag ions migration in the MoS<sub>2</sub> dielectric layer. When a bias was applied on the device, the Ag atoms in the bottom Ag electrode are oxidized to Ag<sup>+</sup> ions by the Joule effect of the electric field. Afterwards, the Ag<sup>+</sup> ions are driven to the top graphene electrode by the applied electric field, leading to the re-distribution and accumulation of the space charge. When reaching the graphene electrode, the Ag cations are gradually reduced to Ag atoms, leading to the Ag filament formation, which facilitates the switch from the HRS to LRS. In contrast, with the applied reverse bias on the device, the Ag atoms of the conductive filament are oxidized to the Ag<sup>+</sup>, which then migrate to the Ag electrode under the electric field. This

leads to the dissolution of the conductive filament, causing the resistance to switch from LRS to HRS. To verify this mechanism, we printed a control device where Gr was used for both electrodes, Fig. S17 (ESI†): no resistance switching behavior is observed, as expected – just a small hysteresis is seen, similar to the one observed in the FS annealed Ag/MoS<sub>2</sub>/Gr device (Fig. S5a, ESI†).

Furthermore, the ECM-based RS mechanism can be easily checked by fitting the *I*-*V* curve of the Ag/MoS<sub>2</sub>/Gr memristor, as shown in Fig. 3a: in the HRS phase, the slope is 1.20 between 0 V to 1 V, showing a linear Ohmic conduction ( $J \propto V$ , where *J* is the current density); the slope increases for *V* > 1 and it is well fitted with the Childs square at high bias (*i.e.*  $J \propto V^2$ ), indicating that the charge transport in the HRS fits well with the space charge limited current (SCLC) model,<sup>33</sup> in agreement with other works.<sup>34</sup> The slope of the *I*-*V* curve of the LRS is 1.22, close to 1, indicating that charge transport conforms to the Ohmic law, in agreement with the filament formation mechanism. Hence, alternative RS models<sup>35</sup> where contribution on the memristic effect was explained by the presence of a Schottky barrier between the MoS<sub>2</sub> flakes and the electrode, with the MoS<sub>2</sub> flakes acting as electron trapping centers, are not valid for our devices.

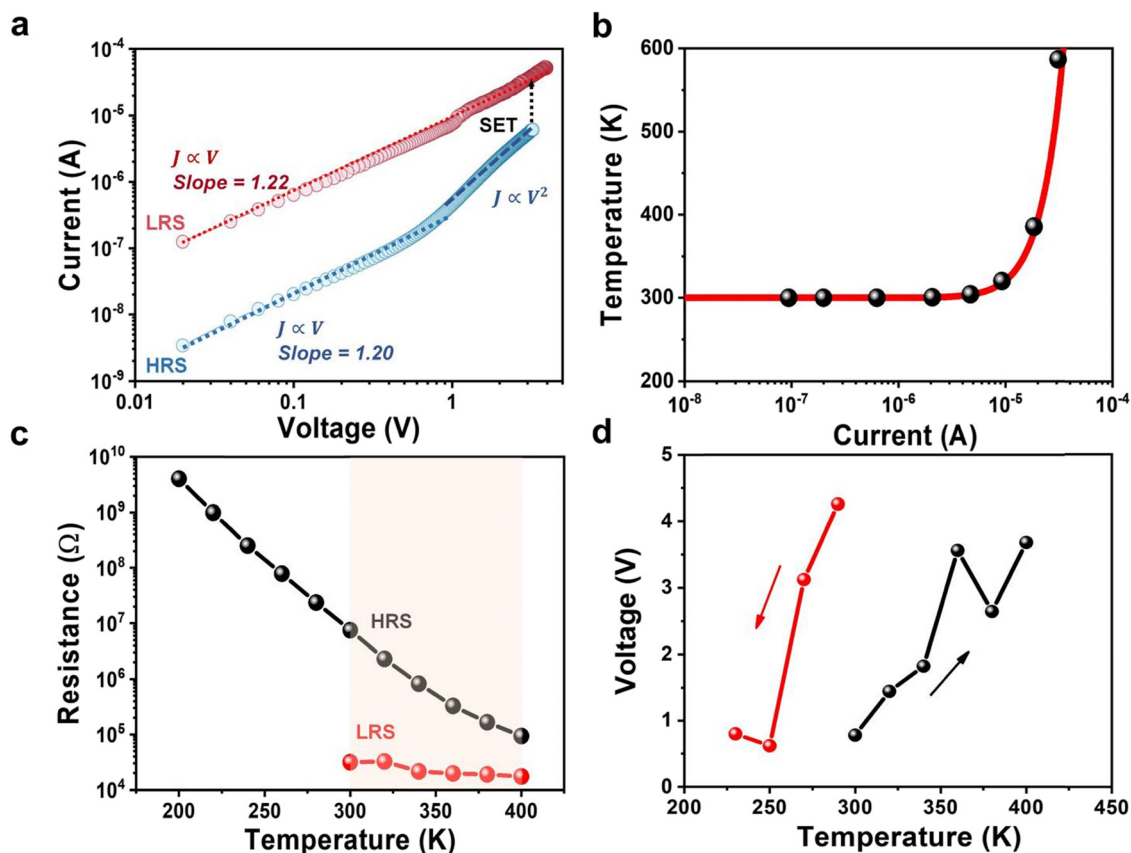


Fig. 3 Resistance switching mechanism of the Ag/MoS<sub>2</sub>/Gr memristor. (a) The positive part of the *I*-*V* curve in double logarithmic coordinates shows Ohmic behaviour in LRS and SCLC behaviour in HRS. (b) Temperature of the conductive filaments as a function of current, calculated using eqn (1). (c) LRS and HRS resistance of the Ag/MoS<sub>2</sub>/Gr memristors as a function of the temperature in the 200–400 K range. (d) Setting voltage as a function of the temperature in the 200–400 K range recorded by increasing (black line) and decreasing temperature (red line).



Finally, following the model proposed in ref. 23, we also extracted the temperature of the conductive filaments using the following equation:<sup>36</sup>

$$T = \frac{f_1 VI}{2\pi t_D k} + T_{\text{amb}} \quad (1)$$

where  $V$  is the applied pulse voltage,  $I$  is the current when applying the pulse voltage (obtained from Fig. S18, ESI<sup>†</sup>),  $T$  is the temperature of the conductive filaments,  $t_D$  is the dielectric thickness (650 nm),  $k$  is the out-of-plane thermal conductivity of MoS<sub>2</sub>,  $T_{\text{amb}}$  is the room temperature, and  $f_1$  is a fitting parameter that is proportional to the power lost at the constriction (*i.e.*,  $I \times V$ ), as shown in Fig. S18b (ESI<sup>†</sup>). The dash lines in Fig. 3b show  $T$  as a function of  $I$ , by using  $t_D = 650$  nm and  $k = 0.3 \text{ W m}^{-1} \text{ K}^{-1}$ .<sup>37</sup> Fig. 3b shows that for  $I > 10 \mu\text{A}$  the temperature starts to increase rapidly, reaching values close to the melting point of the printed Ag nanoparticles ( $\approx 400$  K) in close proximity to the filament.

Moreover, we performed electrical measurements at different temperatures, starting from 200 K and increasing the temperature to 400 K with 20 K steps, which have never been reported for printed memristors. Fig. S19 (ESI<sup>†</sup>), Fig. 3c and d show that memristic behaviour is observed only when the temperature reaches 300 K. Furthermore, Fig. 3c shows that in the HRS, the resistance of the device decreases with the temperature, as expected for a semiconductor.<sup>38</sup> In the LRS, the resistance remains around  $10^4 \Omega$ , independent of the temperature, as

expected for a metal. Moreover, Fig. 3d shows that the setting voltage changes with the temperature. For both the measurements recorded by increasing temperature and decreasing temperature, the setting voltage increases with the temperature. Normally, higher temperature should help silver ions migration, so this observation may indicate a change in the micro-structure of the printed MoS<sub>2</sub> film for increasing temperature, which may hinder the ions migration. Alternatively, this may indicate the presence of another memristic mechanism, in addition to the silver filament, for example related to defects in the MoS<sub>2</sub> film. On the other hand, printed memristors show setting voltage in the range 1–4 V (Fig. 2b), so this variation may simply be within the device-to-device fluctuation range.

To further investigate the origin of the memristic effect observed in the Ag/MoS<sub>2</sub>/Gr device, we used CVD graphene as impermeable barrier,<sup>39–43</sup> by integrating this material (see Experimental and Section S10, ESI<sup>†</sup> for details) onto the silver electrode. CVD graphene is expected to prevent silver ions migration from the electrode to the dielectric. Fig. 4a–d show that although the transfer of graphene is not perfect (*e.g.* some folding and wrinkles are observed, possibly due to the rough silver surface), still it is possible to transfer graphene on a relatively large area with good coverage.

Fig. 4e shows the  $I$ – $V$  characteristics of the Ag/CVD Gr/MoS<sub>2</sub>/Gr device: no memristic behaviour is observed, confirming that the silver ions migration from the bottom Ag electrode to the top graphene electrode is strongly reduced by the presence of

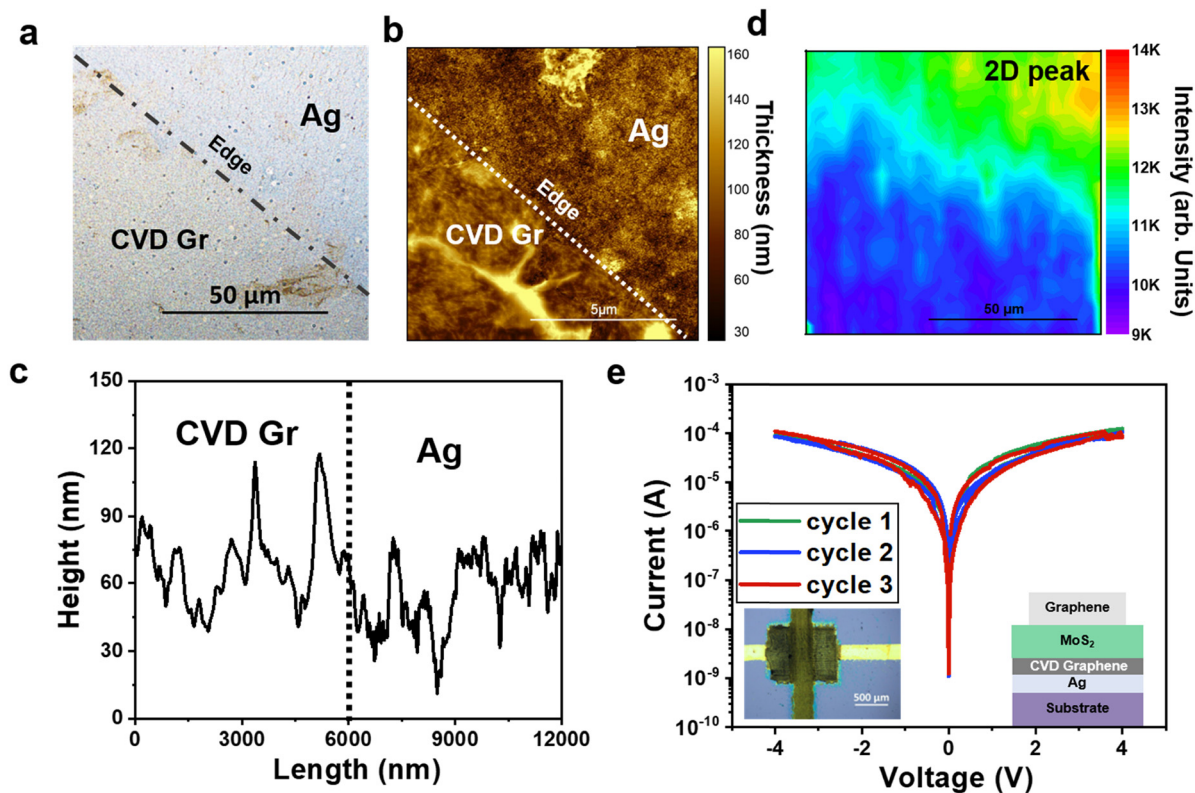


Fig. 4 Ag/MoS<sub>2</sub>/Gr memristors with integration of CVD graphene. (a) Optical image, (b) and (c) AFM image and (d) Raman mapping of the 2D peak intensity of CVD graphene transferred onto the printed Ag electrode. (e)  $I$ – $V$  curves of the Ag/CVD Gr/MoS<sub>2</sub>/Gr device; inset: optical image of the device.











- K. R. Graham, V. Blum, J. M. Luther, M. C. Beard and J. L. Blackburn, *J. Am. Chem. Soc.*, 2023, **145**, 2052.
- 41 X. Zhao, S. Liu, J. Niu, L. Liao, Q. Liu, X. Xiao, H. Lv, S. Long, W. Banerjee, W. Li, S. Si and M. Liu, *Small*, 2017, **13**, 1603948.
- 42 J. S. Bunch, S. S. Verbridge, J. S. Alden, A. M. van der Zande, J. M. Parpia, H. G. Craighead and P. L. McEuen, *Nano Lett.*, 2008, **8**, 2458.
- 43 V. Berry, *Carbon*, 2013, **62**, 1.
- 44 D. Kang and N. Park, *Adv. Mater.*, 2019, **31**, 1805214.
- 45 Y. Hernandez, V. Nicolosi, M. Lotya, F. M. Blighe, Z. Sun, S. De, I. T. McGovern, B. Holland, M. Byrne, Y. K. Gun'Ko, J. J. Boland, P. Niraj, G. Duesberg, S. Krishnamurthy, R. Goodhue, J. Hutchison, V. Scardaci, A. C. Ferrari and J. N. Coleman, *Nat. Nanotechnol.* 2008, **3**, 563.

